Angewandte Chemie

GDCh

Eine Zeitschrift der Gesellschaft Deutscher Chemiker

www.angewandte.de

Akzeptierter Artikel

Titel: Understanding a New NASICON-Type High Voltage Cathode Material for High-Power Sodium-Ion Batteries

Autoren: Mingzhe Chen, Weibo Hua, Jin Xiao, David Cortie, Xiaodong Guo, Enhui Wang, Qinfen Gu, Zhe Hu, Sylvio Indris, Xiaolin Wang, Shulei Chou, and Shixue Dou

Zitierweise: *Angew. Chem. Int. Ed.* 10.1002/anie.201912964
Angew. Chem. 10.1002/ange.201912964

Link zur VoR: http://dx.doi.org/10.1002/anie.201912964
http://dx.doi.org/10.1002/ange.201912964

WILEY-VCH

10.1002/ange.201912964

WILEY-VCH

RESEARCH ARTICLE

Understanding a New NASICON-Type High Voltage Cathode Material for High-Power Sodium-Ion Batteries

Mingzhe Chen,[+] Weibo Hua,[+] Jin Xiao, David Cortie, Xiaodong Guo, Enhui Wang, Qinfen Gu, Zhe Hu, Sylvio Indris, Xiao-Lin Wang, Shu-Lei Chou,* and Shi-Xue Dou

Abstract: The cathode materials for sodium-ion batteries have always been one of the key issues for the ultimate success of large-scale energy storage systems. Here, we introduce a 4.0 V class high-voltage cathode material with a newly recognized sodium superionic conductor (NASICON)-type structure with cubic symmetry (space group $P2_13$), $Na_3V(PO_3)_3N$. We synthesize an N-doped graphene oxide wrapped $Na_3V(PO_3)_3N$ composite with a uniform carbon coating layer, and it shows both excellent rate performance and outstanding cycling stability. Its air/water stability and all-climate performance are carefully investigated in detail. Near-zero volume change (~0.40 %) is clearly observed for the first time based on *in-situ* synchrotron X-ray diffraction, and the *in-situ* X-ray absorption spectra reveal the $V^{3.2+}/V^{4.2+}$ redox reaction with high reversibility. Its three-dimensional sodium diffusion pathways are explicitly demonstrated with distinctive low energy barriers. Higher reversible capacity and a higher working platform can surely be achieved if the electrolyte possesses a wider voltage tolerance window above 4.8 V. Our comprehensive results indicate that this high-voltage new NASICON-type $Na_3V(PO_3)_3N$ composite can be considered as a competitive candidate cathode material for sodium-ion batteries and will receive more extensive attention and studies in the future.

Introduction

The rapid development of cost-efficient large-scale electrical energy storage systems (EESs) has led to remarkable progress on the exploitation of renewable energy resources, such as solar energy, wind energy, and tidal energy in recent years.[1] Although advanced lithium-ion batteries (LIBs) have received great commercial achievements, such as with their application in electric vehicles (EVs) and portable devices with satisfactory energy density and power density levels for EESs, the limited and unevenly distributed nature of lithium resources remains the critical obstacle to their ability to satisfy the urgent demand for battery systems that will be suitable for cost-efficient EESs.[2] Sodium-ion batteries (SIBs) have been extensively investigated as a promising alternative candidate for EESs due to the practically inexhaustible nature of sodium resources.[3] In order to achieve satisfactory performances in SIBs, however, tremendous efforts are still needed to discover or develop more suitable and cost-efficient electrodes, based on a more comprehensive understanding of the mechanisms involved.[4] Therefore, the intrinsic properties of electrodes, especially positive electrodes, play key roles in the overall performance of full SIBs towards real applications in the commercial EES market.[5]

The polyanionic or mixed-polyanion system is considered to be one of the most promising candidates among all types of cathode materials for SIBs, and these types of materials have been systematically investigated in recent years. Their intrinsic robust three-dimensional (3D) frameworks can provide long-term repeated Na^+ ion de-/insertions at various working potentials with small volume change, although their reversible capacities are moderate due to their large mass with high molecular weights.[6] Most of these polyanionic-based materials only possess one- or two dimensional (1D or 2D) sodium diffusion pathways, however, which will result in sluggish sodium diffusion kinetics and inferior rate performance as well.[7] Therefore, the polyanionic-based materials that possess three-dimensional sodium diffusion pathways are ideal cathode candidates since the critical demands of both long-term cycling and high-rate performance can be satisfied at the same time. Sodium superionic conductor (NASICON)-type materials are typical representatives of them.[8] To achieve higher energy density, the working voltage is another important parameter that cannot be neglected. It was found that doping with more electronegative elements is an effective way to enhance the operating potentials.[9]

In this scenario, we are excited to introduce a new family member of the NASICON-type high voltage cathode materials, $Na_3V(PO_3)_3N$, which is of particular interest and utilizes $(PO_3)_3N$ as the main chaining polyanion group.[10] One N^{3-} is shared with three PO_3N tetrahedra, and the presence of N can give rise to strong inductive effects, which will result in enhanced electrostatic repulsion between adjacent V atoms, so that a higher working voltage can be realized during sodium de-/insertion. The pioneering researchers who discovered it have previously investigated isostructural $Na_2Fe_2(PO_3)_3N$ and $Na_3Ti(PO_3)_3N$ materials, and related fundamental understandings have been obtained regarding their intrinsic properties.[11] Kang's group and Casas-Cabana's group almost simultaneously reported some

[*] Dr. M. Chen, Dr. D. Cortie, Dr. E. Wang, Dr. Z. Hu, Prof. X.-L. Wang, Dr. S.-L. Chou, Prof. S.-X. Dou
Australian Institute for Innovative Materials, Institute for Superconducting and Electronic Materials, University of Wollongong, Innovation Campus, Squires Way, North Wollongong, NSW 2522, Australia
E-mail: shulei@uow.edu.au
Dr. W. Hua, Prof. S. Indris
Institute for Applied Materials-Energy Storage Systems (IAM-ESS), Karlsruhe Institute of Technology (KIT), 76344 Eggenstein-Leopoldshafen, Germany.
Dr. J. Xiao
School of Science, Hunan University of Technology, Zhuzhou 412007, P. R. China
Dr. J. Xiao
State Key Laboratory for Superlattices and Microstructures, Institute of Semiconductors, Chinese Academy of Sciences, Beijing 100083, P. R. China
Dr. E. Wang, Prof. X. Guo
College of Chemical Engineering, Sichuan University, Chengdu 610065, P. R. China
Dr. Q.-F. Gu
Australian Synchrotron, 800 Blackburn Road, Clayton, VIC 3168, Australia
[+] These authors contributed equally to this work.

Supporting information for this article is given via a link at the end of the document.

10.1002/ange.201912964

novel discoveries on the undecorated $Na_3V(PO_3)_3N$ material, and they both found that this material only underwent tiny volume change (~ 0.24 %) upon the first Na^+ ion de-/insertion (one electron exchange).[9b, 10] A 4.0 V working platform was recognised, and excellent rate performance was obtained, which corresponds well with its 3D sodium diffusion pathways. Dedicated designs for the material morphology, as well as a more comprehensive understanding of both the chemical and the physical properties of this material under various conditions, are still urgently needed, since the pursuit of higher voltage is the core driving force towards achievable higher energy densities.[12]

Therefore, in this paper, we report a nitrogen-doped graphene oxide (NGO) wrapped $Na_3V(PO_3)_3N$ material with a uniformly carbon coating layer (VN/C@NGO), which demonstrates fast and stable favourable Na storage properties under all-climate temperatures, with nanosized particles to form a composite material with no reduction in its original crystallinity. The dedicated design of the carbon matrix can provide fast electron transport, and the doped nitrogen atoms on NGO can offer possible bonding sites to anchor $(PO_3)N$ tetrahedra, supporting high ionic diffusion capacity.[7b, 13] Satisfactory rate performance was demonstrated, and impressive cycling stability can be achieved under all climate conditions. In addition, the air-stability and water-resistance of this VN/C@NGO material have been proved. We also employed the *in-situ* synchrotron-based X-ray diffraction (XRD) and *in-situ* X-ray absorption spectroscopy (XAS) to better understand its phase variations as well as the valence changes of V during cycling. Density functional theory (DFT) studies and molecular dynamics were used to examine the details of possible sodium diffusion pathways and the vibrational density of states. Our results will shed light on the design and application of these new types of nitridophosphates for high-performance SIBs in the near future.

Results and Discussion

The VN/C@NGO composite was successfully synthesized *via* a simple freeze-drying method following by an annealing procedure at 720 ℃ (Figure S1a) under anhydrous ammonia atmosphere (created by urea in a sealed quartz tube (Figure S1b)). For comparison, the sample that was created without the nitrogen-doped graphene oxide wrapping was denoted as VN/C. The detailed processes for the two samples are summarized in experimental section. In order to obtain the precise phase constituents and atomic arrangements, synchrotron radiation powder diffraction was employed. Figure 1a shows the low Rietveld refinement results on the obtained powder diffraction pattern of the VN/C@NGO sample with a low weighted profile R-factor (R_{wp} = 5.19 %). All the peaks are well fitted with two detected phase: the main phase of $Na_3V(PO_3)_3N$ (marked by blue bars) and the $Na_3V_2(PO_4)_3$ impurity phase (marked by green bars). According to the final Refinement results of both VN/C@NGO and VN/C samples, the proportion of $Na_3V_2(PO_4)_3$ are 2.98 % and 2.16 % in weight, respectively. The trace amount of $Na_3V_2(PO_4)_3$ seems inevitable even after adding a sufficient amount of ascorbic acid as reducing agent, which was also mentioned in previous work.[14] The sample can be indexed to the cubic symmetry within the space group $P2_13$ (a = 9.4490(1) Å), which is very rare in polyanionic systems. Within the 3D robust framework, the $[V(PO_3)_3N]$ units along the *a*-axis each consist of one VO_6 octahedron and three $(PO_3)N$ tetrahedra, and all the $(PO_3)N$ tetrahedra are corner-sharing with respect to the VO_6 octahedra *via* O atoms (insets in Figure 1a). The N atoms are shared with three $(PO_3)N$ tetrahedra, resulting in a strong inductive effect towards adjacent V atoms.

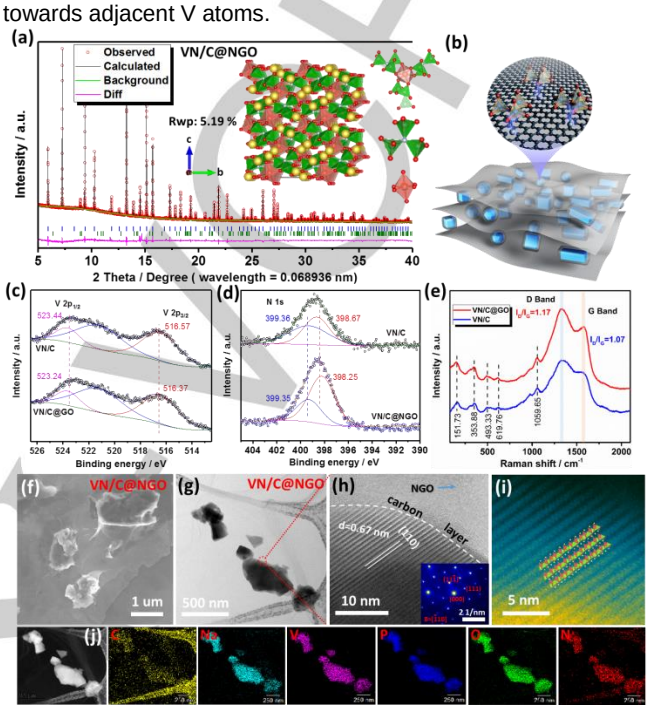

Figure 1. (a) Rietveld refinement of VN/C@NGO. The blue bars below the diffraction pattern represent the $Na_3V(PO_3)_3N$ phase and the green bars indicate the $Na_3V_2(PO_4)_3$ phase. The insets contain schematic representations of $Na_3V(PO_3)_3N$, the $V(PO_3)_3N$ group, and VO_6 octahedra. (b) Schematic illustration of the carbon matrix of VN/C@NGO composite. XPS spectra of both samples for (c) V 2p orbitals, and (d) N 1s orbitals. (e) Raman spectra from 100 cm^{-1} to 2100 cm^{-1}. (f) SEM image and (g) TEM image of VN/C@NGO. (h) Bright field (BF) image of VN/C@NGO with uniform carbon layer and wrapping with nitrogen-doped graphene oxide; inset: selected area electron diffraction (SAED) pattern. (i) High-angle annular dark field (HAADF) image from aberration-corrected scanning TEM (STEM), and the corresponding crystal structure as inset. (j) STEM-energy dispersive spectroscopy (EDS) mapping results for detected elements: C, Na, V, P, O, and N.

The VN/C sample also exhibited good crystallinity with the symmetric of $P2_13$ (as shown in Figure S2). The detailed summarized atomic site information for VN/C@NGO and VN/C samples can be found in Table S1 and Table S2, respectively. A schematic illustration of the specially designed carbon matrix of the VN/C@NGO sample is shown in Figure 2b. The carbon matrix can enhance the electron transport and the doped N on graphene oxide can provide extra bonding sites for bulk materials. Figure S3 shows the paramagnetic properties of the field-dependent magnetization curve (*M-H*) and the temperature-dependence of the magnetic susceptibility ((*M*/*H*-*T*) and the inverse magnetic susceptibility (χ^{-1}-*T*) of the VN/C@NGO sample, probing the spin state of V. The calculated value for the effective magnetic moment

10.1002/ange.201912964

WILEY-VCH

(μ_{eff}) is 4.67 μ_B/V per formula unit, which is close to theoretical value of 4.50 μ_B/V per formula unit for the high-spin V^{3+} state (d^2, t_{2g}^2, $S = 0$).[15]

The carbon contents of the VN/C@NGO and VN/C samples were detected to be 5.54 % and 4.34 %, respectively (Figure S4). Further characterizations were carried out with X-ray photoelectron spectroscopy (XPS) and Raman spectroscopy. Figure 1c and d shows the surface chemical compositions of the V and N elements. It can be seen that there are almost no obvious differences for V $2p_{1/2}$ and $2p_{2/3}$, and their bonding energies are close to the theoretical values for trivalent vanadium. Pyridinic N and graphitic N contribute to the N 1s spectra of both samples,[16] and the peak intensity of VN/C@NGO is higher than that of VM/C, indicating that the nitrogen concentration on the surface is increased by introducing the N-doped graphene oxide. The Raman spectrum in the range from 100 cm^{-1} to 2100 cm^{-1} is displayed in Figure 1e. The observed small peaks located at 151.73 cm^{-1} and 353.88 cm^{-1} can be assigned to the stretching/bending vibrations of $(PO_3)N$ tetrahedra, while peaks at 493.33 cm^{-1}, 619.76 cm^{-1}, and 1059.65 cm^{-1} can be considered as the bending/stretching motions of the VO_6 octahedra. The intensity ratio of the D band (I_D) to the G band (I_G) of VN/C@NGO is slightly higher than that of VN/C. The D band normally reflects the defects, edges, and structural disorder, while the G band commonly represent the E_{2g} mode of sp^2 carbon layers.[6b, 17] This phenomenon indicates that the N-doped GO possesses more defects, which can favour the electron conductivity as well as possible bonding sites.[18] Also, from the Fourier transform infrared (FT-IR) spectra in Figure S5, both symmetric and asymmetric bending/stretching modes of the tetrahedra and octahedra can be found near 1000 cm^{-1}.

Scanning electron microscope (SEM) and scanning transmission electron microscope (STEM) images are shown in Figure 1 and Figure S6 for both samples. Figure 1f and g clearly show the wrapped N-dope graphene oxide on as-obtained $Na_3V(PO_3)_3N$ particles with an average size of 1 µm. The morphology of VN/C samples is shown in Figure S6a and b. The carbon layer is uniformly coated on both VN/C@NGO and VN/C particles (Figure 1h and Figure S6c) with thickness around 3-5 nm. The closely wrapped N-doped GO also can be observed near the particles, and its thickness was measured to be 2-3 nm on average (Figure S7). The (110) and (310) lattice planes were measured and confirmed for the VN/C@NGO and VN/C samples, respectively. The insets in Figure 1h and Figure S6d are the corresponding selected area electron diffraction (SAED) patterns, implying that well-crystallized structures of both samples were obtained with space group of $P2_13$. From the high angle annular dark field (HAADF) – STEM images in Figure 1i and Figure S6d, the lattice fringes of both samples can be clearly observed with the identified atom arrangements represented above. The STEM-based energy dispersive spectroscopy (EDS) mapping results for both samples are displayed in Figure 1j and Figure S6e, respectively, where the elements Na, V, P, O, N, and C coexist and are uniformly distributed, which is in satisfactory agreement with the refined powder diffraction data. The element N is also homogeneously distributed on the graphene oxide, indicating the proposed N-doped graphene oxide was well-prepared.

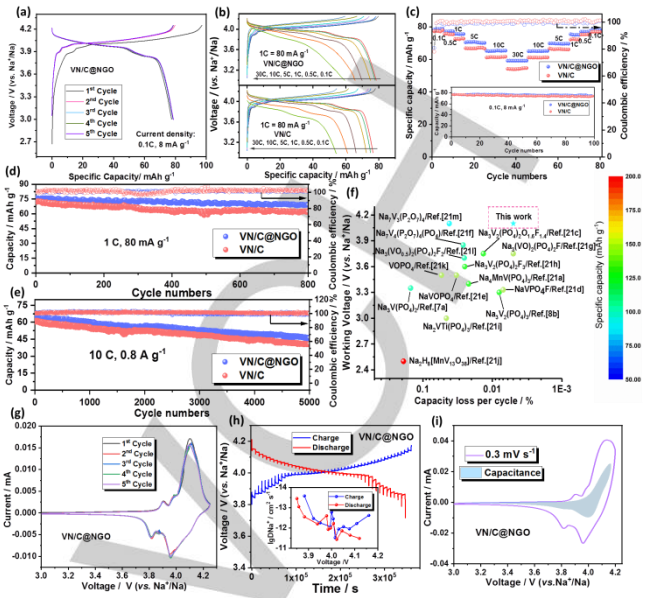

Figure 2. (a) Charge-discharge curves for the first 5 cycles of VN/C@NGO electrode in the voltage window of 3.0 - 4.25 V (current density: 0.1 C, 8 mA g^{-1}). (b) Charge-discharge profiles at different C-rates for both the VN/C@NGO and the VN/C electrodes. (c) Rate capability of both samples from 0.1 C to 30 C. The inset is the low current cycling performance at 0.1 C within 100 cycles. Long-term cycling stability of both electrodes at (d) 1 C for 800 cycles and (e) 10 C for 5000 cycles. (f) 2D comparison of all representative vanadium-based polyanionic cathode materials regarding their cyclability, working potential, and cycle numbers for SIBs. (g) Cyclic voltammetry (CV) curves for initial five cycles of VN/C@NGO electrode. (h) Galvanostatic intermittent titration technique (GITT) curves of VN/C@NGO electrode for both charge and discharge processes (after 10 cycles, current density: 0.1 C); the inset shows the log of the sodium ion diffusion coefficient as a function of voltage. (i) The calculated capacitance contribution (marked as shadowed area) from the CV profile of VN/C@NGO at a scan rate of 0.3 mV s^{-1}.

The electrochemical performances of both the VN/C and the VN/C@NGO samples were examined in coin cells with Na metal as the counter electrode. The electrolyte used in this paper consisted of 1 M $NaClO_4$ dissolved in ethylene carbonate/propylene carbonate (EC/PC, 1:1 by volume with 5 vol. % fluoroethylene carbonate (FEC) as additive agent).[19] The loading mass was controlled to be ~ 2.5 mg cm^{-2} for all electrochemical tests. The $Na_3V(PO_3)_3N$ material shows a typical 4 V class working platform, as shown in Figure 2a. The initial cycle Coulombic efficiency is around 80 %, which is possibly due to the pre-oxidation of vanadium in this nitrogen-containing system, which will be analysed and discussed later. The VN/C@NGO electrode can deliver specific capacities of 78.9 mAh g^{-1} at 0.1 C (1 C = 80 mA g^{-1}) and 59.2 mAh g^{-1} at 30 C without any obvious large polarization (Figure 2b). The polarization of the VN/C electrode is slightly larger but remains acceptable. Excellent rate capabilities of both samples are demonstrated in Figure 2c, which are entirely comparable with the known NASICON-structured polyanionic materials, such as the well-studied $Na_3V_2(PO_4)_3$.[20] The inset in Figure 2c presents the cyclability of both samples at low current density (0.1 C) for 100 cycles, and almost no capacity drops were observed. In

10.1002/ange.201912964

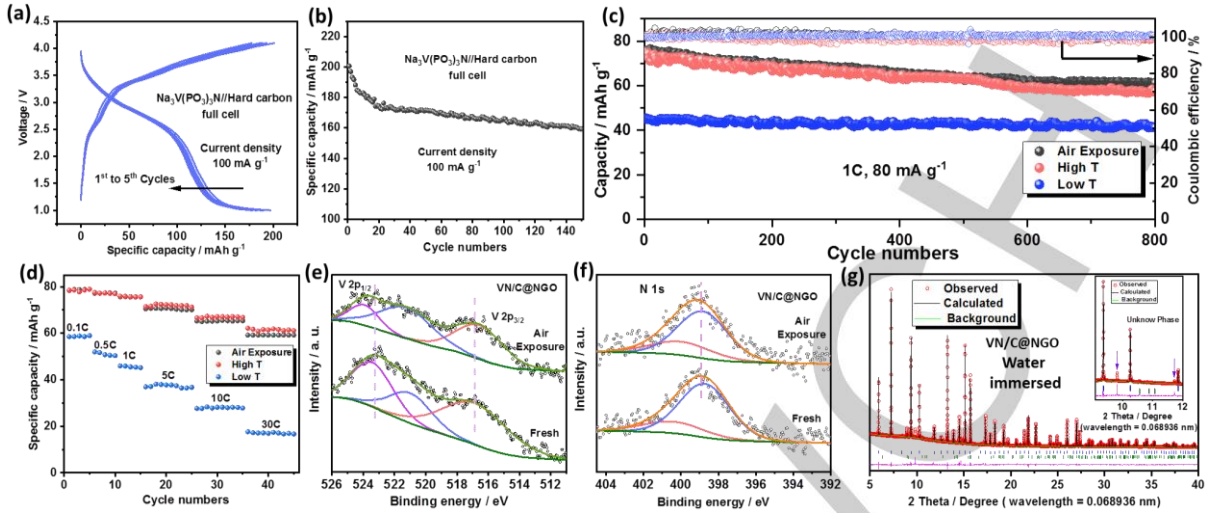

Figure 3. (a) Voltage profiles of $Na_3V(PO_3)_3N$//Hard carbon full cell for the first five cycles at current density of 100 mA g^{-1} (based on the anode). (b) Cycling stability of the $Na_3V(PO_3)_3N$//Hard carbon full cell for 150 cycles. (c) Comparison of the cyclability of VN/C@NGO sample subject to air exposure (3 months), high temperature (50 ℃), and low temperature (-15 ℃) over 800 cycles. (d) Rate capabilities of air exposure, high temperature, and low temperature VN/C@NGO samples. (e) V 2p and (f) N 1s XPS spectra of VN/C@NGO sample in the fresh state and after exposure to air for three months. (g) Powder diffraction and Rietveld refinement results for VN/C@NGO sample after immersion in water, with the inset showing an enlargement of the peak for an unknown phase.

addition, the long-term cyclability of both electrodes was also measured at both 1 C (800 cycles) and 10 C rates (5000 cycles), and capacity retention of 91.0 % and 75.9 % could be achieved, respectively. What is worth mentioning is that there is almost no mid-voltage decay within 800 cycles, which is very important for maintaining the overall energy density retention in practical use. The VN/C electrode shows similar trends of capacity degradation in these cycling tests, indicating that the N-doped GO is the only reason for the electrochemical discrepancy. We further examined the electrode after 5000 cycles, and no obvious cracks were observed, while the lattice fringes of the (110) plane could still be clearly observed. The SAED pattern also shows the well-crystallized structure, and all the detected elements, C, Na, V, P, O and N, are homogeneously distributed (Figure S8), indicating its robust framework nature even after a thousand cycles of sodium de-/insertion. In Figure 2f, we compare all the vanadium-based polyanionic cathode materials regarding their cyclability, working potential, and corresponding capacities for SIBs.[8b, 21] The $Na_3V(PO_3)_3N$ material presented in this work has a high voltage platform and balanced cycling stability, although its current achievable capacity is relatively low due to the restricted electrolyte voltage window. The potential for a second sodium de-/insertion is calculated to be around or above 5 V, which is far beyond the stable voltage window of current commercial electrolytes.

The cyclic voltammetry (CV) curves for the initial five cycles of VN/C@NGO electrode are exhibited in Figure 2g. It can be seen that unlike those alluaudite-type polyanions, this $Na_3V(PO_3)_3N$ material does not show any changes in the cation arrangement or phase in the initial cycle, which is in favour of long-term cycling stability with only a very small volume change. No significant difference can be found between the pristine electrodes of VN/C@NGO and VN/C in the electrochemical impedance spectroscopy (EIS) results but after one cycle, the interface resistance of VN/C@NGO witnessed a large decline, which can be attributed to the formation of the solid-electrolyte interphase (SEI) layer (Figure S9). The galvanostatic intermittent titration technique (GITT) was carried out in a coin cell after reaching its thermal equilibrium (10 cycles) (Figure 2h). A solid-solution reaction mechanism can be recognised based on the one electron transfer process. Sodium diffusion coefficients for VN/C@NGO were calculated based on the GITT results and are displayed in the inset in Figure 2h within the main range from 10^{-13} to 10^{-11} cm^2 s^{-1}, which is completely comparable to those of well-known NASICON-type materials. The details for this calculation can be found in Figure S10. What is more, the capacitance contribution was calculated from a series of different CV scan rates (Figure S11). It provides convincing evidence that both the faradic and non-faradic processes always coexist during cycling and that they both have positive effects on the ultimate electrochemical performance. The faradic process (oxidation/reduction reaction) can provide a fix working potential, while the non-faradic process can help the fast charge transitions related to the double-layer effect (normally regarded as pseudocapacitance). The capacitance contribution is shown in Figure 2i (22.3 % of the total current) with the values for the *b* parameter around 0.70 with four identified redox peaks. This can be considered as another key factor behind the excellent electrochemical performance of VN/C@NGO electrode.

We further tested the air stability and all-climate performances of $Na_3V(PO_3)_3N$ material with a view towards its real applications. We first prepared a $Na_3V(PO_3)_3N$//Hard carbon full cell, and the results are shown in Figure 3a-b. The hard carbon was purchased from KURARAY Co., Ltd., Japan (Type 2), and both the capacity and current density values are based on the anode part. An initial reversible specific capacity of ~200 mAh g^{-1} could be achieved at the current density of 100 mA g^{-1} in the voltage window of 1.5- 4.0

10.1002/ange.201912964

WILEY-VCH

V. Capacity retention of 80 % was achieved after 150 cycles with high Coulombic efficiency

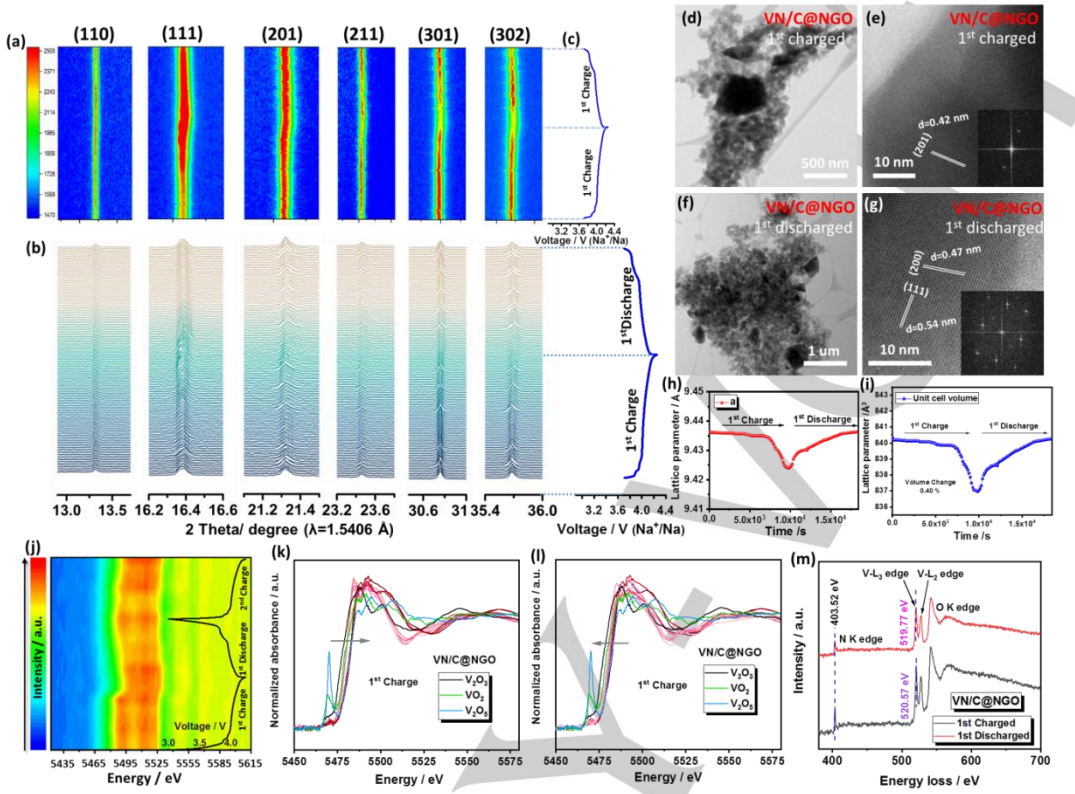

Figure 4. (a) 2D contour plot and (b) stacked synchrotron-based *in-situ* XRD patterns, and (c) corresponding electrochemical profile of the initial cycle of VN/C@NGO electrode. (d) and (f) TEM images of the 1st cycle charged and 1st cycle discharged $Na_3V(PO_3)_3N$ electrode; (e) and (g) HRTEM images of the 1st cycle charged and 1st cycle discharged $Na_3V(PO_3)_3N$ electrode. The insets are the fast Fourier transform (FFT) patterns. (h) Variations of crystal parameter of *a*, and (b) the corresponding unit cell volume change for the initial cycle. (j) *In-situ* XANES spectra at the V K-edge of $Na_3V(PO_3)_3N$ material (2D contour plot) of charge-discharge-charge profile. (k) and (l) Charge/discharge process V K-edge XANES spectra. (m) The electron energy loss spectroscopy (EELS) spectra of the 1st cycle charged and 1st cycle discharged electrodes of $Na_3V(PO_3)_3N$ material.

near 100 %. In should be pointed out that, since the initial cycle Coulombic efficiency (ICE) of hard carbon is relatively low, the anodes in the full cell were pre-cycled. From Figure 3c, it can be seen that the VN/C@NGO samples that were subjected to air exposure and high-temperature showed no obvious difference (90.3 % and 86.4 %, respectively), while the low-temperature one showed more stable cycling performance but lower specific capacity (92.3 %). The C-rate performances in Figure 3d show the similar tendencies. The satisfactory high/low-temperature properties cannot be achieved without the sturdy framework of its 3D open polyanionic cubic structure as well as 3D sodium diffusion pathways, which will be explored and discussed later. From the demonstrated results above, it can be deduced that this $Na_3V(PO_3)_3N$ material can work under all sorts of different conditions, which is very promising for real applications of SIBs in the commercial market. We further examined the details of the fresh sample and the air exposed one to gain a deeper understanding of air stability properties. We first employed the STEM technique to obtain the crystal details. Figure S12 shows that the air exposed VN/C@NGO sample still maintains good crystallinity and a uniform carbon layer as well. The SAED pattern also exhibits a single phase crystalline character. In addition, the STEM-EDS mapping results indicate that all the relevant elements remain homogeneously distributed. In Figure 3e and f, the V 2p and N 1s XPS spectra were deconvoluted, and it was found that there was no significant discrepancy or shift in position between the fresh and the air exposed samples, which means that the surface chemical surroundings are almost the same for both samples. What is more, we further immersed the $Na_3V(PO_3)_3N$ material in water for 1 h with ultrasonication to test its solubility. To our surprise, the water immersed sample still possesses high crystallinity (as shown in Figure 3g) with very good Rietveld refinement results except for a raised trace amount of unknown phase (as illustrated in the inset in Figure 3g). We also employed the STEM technique to determine the reasons. It can be seen in Figure S13 that the NGO was removed by ultrasonication and that the $Na_3V(PO_3)_3N$ material is insoluble, although phase segregation can be observed in the HAADF image. It can be possibly deduced that the phase transition on the surface may have hindered more crystal change in the bulk, although the generated new phase is currently unknown. The SAED and EDS data demonstrate that the whole material is still well crystallized even after being immersed in water for 1 hour. Its water stability is quite uncommon in the case of pyrophosphates, which usually

10.1002/ange.201912964

suffer from surface electrochemical degeneration.[22] This phenomenon also indicates that the P-N bond is highly hybridized in $Na_3V(PO_3)_3N$ and can be possibly used in other types of polyanionic materials. Therefore, this material is worthy of being investigated as a cathode material for aqueous SIB systems as well.

In order to obtain more precise phase transition and valence variation information, both *in-situ* synchrotron-based XRD patterns and X-ray absorption spectra (XAS) were collected at the Australian Synchrotron and the P64 beamline at DESY, Germany, respectively. The wavelength was changed manually to 1.5406 Å for more visual comparison. A whole pattern over the full range from 5° to 90° (λ = 1.5406 Å) is shown in Figure S14. From Figure 4a and b, it can be clearly seen that this material almost underwent a zero-strain phase change during the initial cycle. Major reflections such as 110, 111, and 201 were easily identified and showed almost no shifts during charge and discharge. From the 2D contour plot, almost imperceptible peak shifts were observed and measured. The TEM and HRTEM images of fully charged and fully discharged $Na_3V(PO_3)_3N$ electrode are displayed in Figure 4d-g. Lattice fringes for the (201), (111), and (200) planes are clearly observed and identified, indicating that the high crystallinity is well maintained throughout all the electrochemical procedures. The remaining Na^+ ions in the crystal structure (around 67 %) can be regarded as the key factor for the zero-strain process. Kang's group previously explained that the reduced electrostatic attraction created by larger vacant Na1 sites can compete with the shrinking V-O bonds.[10] Also, the unusual cubic symmetry can prevent possible cation displacements. We carefully measured the tiny crystal parameter and volume changes and a total 0.40 % volume change was identified, which is thoroughly negligible compared to other types of cathode materials (Figure 4h and i). This zero-strain topotactic single phase transition of $Na_3V(PO_3)_3N$ electrode is interesting and will received more investigation from various aspects. Furthermore, *in-situ* X-ray absorption near-edge structure (XANES) spectra are exhibited in Figure 4j-l. V_2O_3, VO_2 and V_2O_5 were used as references for the valences of V^{3+}, V^{4+}, and V^{5+}, respectively. The 2D contour plot of the normalized XANES spectra shows obvious reversible variations in the valence of V around 5510 eV in the illustrated cycles. Figure 4k shows the XANES spectra shifting towards higher energy during charge and shifting towards lower energy during discharge, which exhibits the excellent valence reversibility of V in $Na_3V(PO_3)_3N$ material. We carefully examined and simulated the valence of V during the 1st cycle charge and discharge processes, and we found that the valence of V changes with ~ $V^{3.2+}/V^{4.2+}$, not as the supposed V^{3+}/V^{4+} redox. This finding provides a good explanation for the relatively low ICE of $Na_3V(PO_3)_3N$ illustrated in Figure 2a. The same phenomenon was observed by Reynaud *et al.*[9b] and Zhang *et al.*[14] previously, indicating that the relative low ICE is largely due to the pre-oxidation of V from +3 in the initial charge process. Besides, the pre-edge of the V K-edge during charging also exhibits discernible variation with reversible peak shifts, although the pre-edge peaks are not similar to those in the references, which can be ascribed to the different fingerprint information

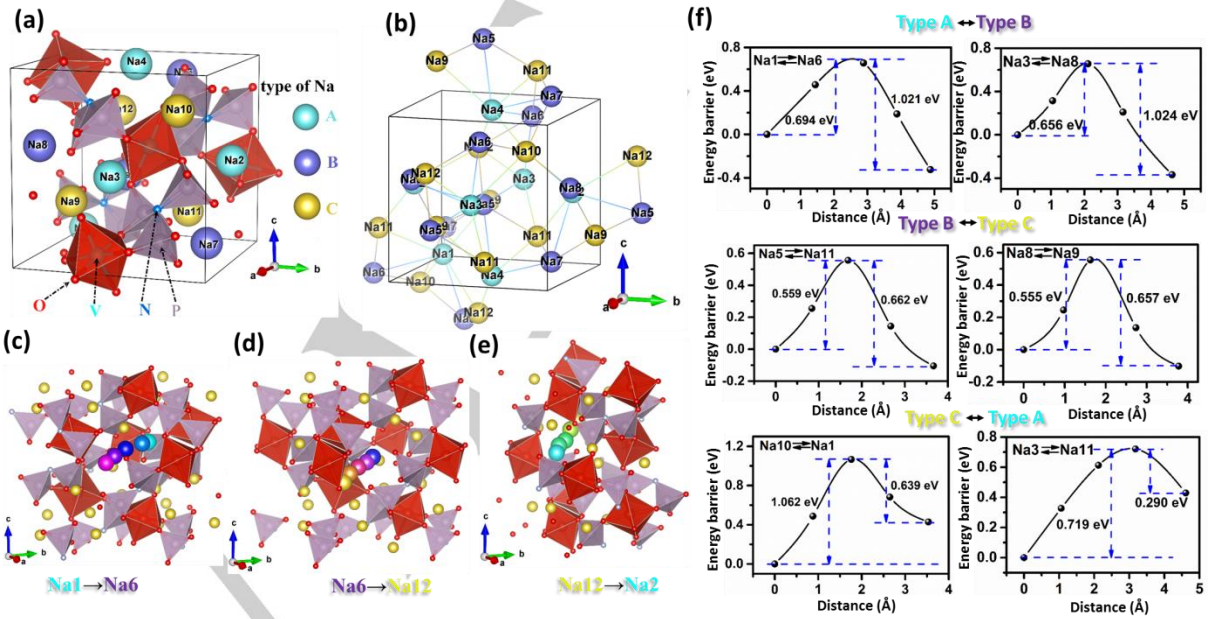

Figure 5. **Schematic illustrations of Crystal structure, possible Na^+ ion diffusion pathways, and corresponding migration energy barriers in a single unit.** (a) and (b) Illustrations of crystal structure of $Na_3V(PO_3)_3N$ material with three different types of Na^+ ions. Calculated Na^+ ion pathways of (c) the A to B type, (d) the B to C type, and (e) the C to A type. (f) The migration energy barriers within the different Na^+ ion groups.

on VO_6 octahedra.[9a, 21i] In Figure 4m, we also employed the electron energy loss spectroscopy (EELS) technique to probe the valence variations of V. The areas for the EELS tests are displayed in Figure S15. It can be found that corresponding shifts of the V-L_3 edge occur from 520.57 eV to 519. 77 eV, which indicates charge compensation in the 3*d* orbital of V. No variations of the N K-edge were found, meaning that the strongly hybridized N atoms were not involved in the electrochemical reactions. The

XPS results in Figure S16 also confirmed similar conclusions to those observed in the EELS tests. The full theoretical specific capacity of $Na_3V(PO_3)_3N$ is be expected to be achieved with significant breakthroughs in high-voltage durable electrolytes, since the V^{4+}/V^{5+} redox couple was not fully involved.

In order to fully understand the intrinsic properties of the unique cubic structure that possesses excellent C-rate performance, a density functional theory (DFT) study was employed to probe the migration energy barriers of Na^+ within different Na^+ ion types. We first found that all of the 12 Na^+ ions in a single crystal unit can be divided into three different types, based on their individual binding energies (namely A, B, and C types). The details for the three types of Na^+ ions and the corresponding calculation method are shown in Table S3. In Figure 5a and b, various images of $Na_3V(PO_3)_3N$ material with three different types of Na^+ ions are displayed. Sodium diffusion between the same types of Na^+ ion are possible except for the A to A type, since the O atom will block the pathway. The energy barriers to sodium diffusions between B to B and C to C types are all below 0.5 eV according to calculations. The B to B type along the *c* direction has the lowest energy barrier and shortest diffusion distance, so that this type is likely to be first extracted during the charging process. Then, we performed the calculations between different types of Na^+ ions, which are equivalent to 3D diffusion pathways because the *a*, *b*, and *c* orientations are all involved. From Figure 5f, it can be seen that the energy barriers are all below 1.1 eV, which are all highly active diffusion pathways for $Na_3V(PO_3)_3N$ material, supporting solid evidence for this newly recognized NASICON-type structure with 3D sodium diffusion pathways.[23] Also, according to a previous report, the $Na_3V(PO_3)_3N$ material possesses high ionic conductivity,[24] which is of the same order as well-recognized NASICON-type $Na_3V_2(PO_4)_3$ at various temperatures. The vibrational density of states results presented in Figure S17 for this $Na_3V(PO_3)_3N$ material also indicate the highly mobility of sodium ions at 1-10 THz (equivalent to 40-400 K), which agrees well with the all-climate performance reported in Figure 3. Considering the high voltage platform, long-term cycling stability, outstanding C-rate capability, and all-climate performance, we believe that this newly recognized NASICON-type $Na_3V(PO_3)_3N$ material is a highly competitive candidate among all the different types of cathode materials for real application in SIBs in large-scale EESs with the potential to reach even higher energy density once the electrolyte can sustain wider voltage windows in the near future.

Conclusion

In summary, we have successfully synthesized $Na_3V(PO_3)_3N$ material, a new member of the NASICON family with a well-designed carbon matrix network. This new cathode material possesses a 4 V-class redox potential, and excellent rate performance of 78.9 and 59.2 mAh g^{-1} at 0.1 C and 30 C, respectively, were achieved with impressive cycling stability up to 5000 cycles (capacity retention of 75.9 % at 10 C). Its air/water stability and all-climate (-15 °C and 50 °C) performance were investigated, and satisfactory electrochemical properties and phase stability were obtained and confirmed. A negligible volume change of 0.40 % was clearly observed, based on *in-situ* synchrotron XRD observations, leading to its designation as a virtually zero strain cathode material. The *in-situ* XANES results revealed reversible V-K edge shifts according to the simulated $V^{3.2+}/V^{4.2+}$ redox couple, and the EELS results showed that N was not involved in the electrochemical reactions. A GITT study revealed high sodium diffusion coefficients, and its NASICON-type structure and 3D sodium diffusion pathways were carefully calculated *via* a DFT study to have low energy barriers. Our comprehensive studies indicate that this high-voltage polyanionic $Na_3V(PO_3)_3N$ material is very promising with on-hold potential to reach higher energy density, and it should receive more extensive attention towards its real application in SIBs in the near future.

Acknowledgements

This work is supported by Australian Research Council (ARC DP160102627) and the Australian Renewable Energy Agency (ARENA S_4) projects, the National Natural Science Foundation of China (Grant Nos. 11704114, 61427901), the Hunan Provincial Natural Science Foundation of China (Grant No. 2018JJ3110), the Scientific Research Fund of the Hunan Provincial Education Department of China (Grant No. 17C0462), and a China Postdoctoral Science Foundation Funded Project (Grant No. 2017M620872). The authors would like to thank Dr. Gilberto Casillas-Garcia for the STEM technique support and Dr. Tania Silver for critical reading of the manuscript. Parts of the experiments were carried out at the Powder Diffraction Beamline, Australian Synchrotron, and parts of the experiments were carried out at the P64 beamline at the DESY Synchrotron, Hamburg, Germany.

Conflict of interest

The authors declare no conflict of interest.

Keywords: high voltage • new NASICON-type • 3D pathways • zero-strain • sodium-ion battery

[1] a) M. Armand, J.-M. Tarascon, *Nature* **2008**, *451*, 652-657; b) B. Dunn, H. Kamath, J.-M. Tarascon, *Science* **2011**, *334*, 928-935.

[2] Z. P. Cano, D. Banham, S. Ye, A. Hintennach, J. Lu, M. Fowler, Z. Chen, *Nature Energy* **2018**, *3*, 279-289.

[3] J. Y. Hwang, S. T. Myung, Y. K. Sun, *Chem. Soc. Rev.* **2017**, *46*, 3529-3614.

[4] N. Yabuuchi, K. Kubota, M. Dahbi, S. Komaba, *Chem. Rev.* **2014**, *114*, 11636-11682.

[5] a) M. Chen, Q. Liu, S.-W. Wang, E. Wang, X. Guo, S.-L. Chou, *Adv. Energy Mater.* **2019**, *9*, 1803609; b) M. Chen, L. Chen, Z. Hu, Q. Liu, B. Zhang, Y. Hu, Q. Gu, J.-L. Wang, L.-Z. Wang, X. Guo, S.-L. Chou, S.-X. Dou, *Adv. Mater.* **2017**, 29, 1605535; c) K. Hurlbutt, S. Wheeler, I. Capone, M. Pasta, *Joule* **2018**, *2*, 1950-1960; d) C. Vaalma, D. Buchholz, M. Weil, S. Passerini, *Nature Rev. Mater.* **2018**, *3*, 18013; e) Z. Hu, Z. Tai, Q. Liu, S.-W. Wang, H. Jin, S. Wang, W. Lai, M. Chen, L. Li, L. Chen, Z. Tao, S.-L. Chou, *Adv. Energy Mater.* **2019**, *9*, 1803210; f) W. Ding, L. Hu, J. Dai, X. Tang, R. Wei, Z. Sheng, C. Liang, D. Shao, W. Song, Q. Liu, M. Chen, X. Zhu, S. Chou, X. Zhu, Q. Chen, Y. Sun, S. X. Dou, *ACS Nano* **2019**, *13*, 1694-1702; g) M. Chen, E. Wang, Q. Liu, X. Guo, W. Chen, S.-L. Chou, S.-X. Dou, *Energy Storage Mater.* **2019**, *19*, 163-178.

[6] a) T. Yuan, Y. Wang, J. Zhang, X. Pu, X. Ai, Z. Chen, H. Yang, Y. Cao, *Nano Energy* **2019**, *56*, 160-168; b) M. Chen, W. Hua, J. Xiao,

D. Cortie, W. Chen, E. Wang, Z. Hu, Q. Gu, X. Wang, S. Indris, S. L. Chou, S. X. Dou, *Nat. Commun.* **2019**, *10*, 1480.

[7] a) J. Kim, G. Yoon, H. Kim, Y.-U. Park, K. Kang, *Chem. Mater.* **2018**, *30*, 3683-3689; b) M. Chen, D. Cortie, Z. Hu, H. Jin, S. Wang, Q. Gu, W. Hua, E. Wang, W. Lai, L. Chen, S.-L. Chou, X.-L. Wang, and S.-X. Dou, *Adv. Energy Mater.* **2018**, *8*, 1800944.

[8] a) E. Wang, W. Xiang, R. Rajagopalan, Z. Wu, J. Yang, M. Chen, B. Zhong, S. X. Dou, S. Chou, X. Guo, Y.-M. Kang, *J Mater. Chem. A* **2017**, *5*, 9833-9841; b) E. Wang, M. Chen, X. Liu, Y. Liu, H. Guo, Z. Wu, W. Xiang, B. Zhong, X. Guo, S. Chou, S.-X. Dou, *Small Methods* **2018**, *3*, 1800169.

[9] a) G. Yan, S. Mariyappan, G. Rousse, Q. Jacquet, M. Deschamps, R. David, B. Mirvaux, J. W. Freeland, J. M. Tarascon, *Nat. Commun.* **2019**, *10*, 585; b) M. Reynaud, A. Wizner, N. A. Katcho, L. C. Loaiza, M. Galceran, J. Carrasco, T. Rojo, M. Armand, M. Casas-Cabanas, *Electrochem. Commun.* **2017**, *84*, 14-18.

[10] J. Kim, G. Yoon, M. H. Lee, H. Kim, S. Lee, K. Kang, *Chem. Mater.* **2017**, *29*, 7826-7832.

[11] J. Liu, D. Chang, P. Whitfield, Y. Janssen, X. Yu, Y. Zhou, J. Bai, J. Ko, K.-W. Nam, L. Wu, Y. Zhu, M. Feygenson, G. Amatucci, A. Van der Ven, X.-Q. Yang, P. Khalifah, *Chem. Mater.* **2014**, *26*, 3295-3305.

[12] a) Z. Dai, U. Mani, H. T. Tan, Q. Yan, *Small Methods* **2017**, *1*, 1700098; b) B. Senthilkumar, C. Murugesan, L. Sharma, S. Lochab, P. Barpanda, *Small Methods* **2019,** *3*, 1800253; c) Y. You, A. Manthiram, *Adv. Energy Mater.* **2018**, *8*, 1701785.

[13] a) P. Ge, H. Hou, S. Li, L. Yang, X. Ji, *Adv. Funct. Mater.* **2018**, *28*, 1801765; b) W. Wang, X. Liu, Q. Xu, H. Liu, Y.-G. Wang, Y. Xia, Y. Cao, X. Ai, *J Mater. Chem. A* **2018**, *6*, 4354-4364.

[14] H. Zhang, D. Buchholz, S. Passerini, *Energies* **2017**, *10*, 889.

[15] B. Wen, Q. Wang, Y. Lin, N. A. Chernova, K. Karki, Y. Chung, F. Omenya, S. Sallis, L. F. J. Piper, S. P. Ong, M. S. Whittingham, *Chem. Mater.* **2016**, *28*, 3159-3170.

[16] W. Shen, H. Li, Z. Guo, C. Wang, Z. Li, Q. Xu, H. Liu, Y. Wang, Y. Xia, *ACS Appl. Mater. Interfaces* **2016**, *8*, 15341-15351.

[17] Z. Hu, Q. Liu, K. Zhang, L. Zhou, L. Li, M. Chen, Z. Tao, Y. M. Kang, L. Mai, S. L. Chou, J. Chen, S. X. Dou, *ACS Appl. Mater. Interfaces* **2018**, *10*, 35978-35983.

[18] Y. Ma, Q. Guo, M. Yang, Y. Wang, T. Chen, Q. Chen, X. Zhu, Q. Xia, S. Li, H. Xia, *Energy Storage Mater.* **2018**, *13*, 134-141.

[19] J. Y. Jang, H. Kim, Y. Lee, K. T. Lee, K. Kang, N.-S. Choi, *Electrochem. Commun.* **2014**, *44*, 74-77.

[20] R. Gao, R. Tan, L. Han, Y. Zhao, Z. Wang, L. Yang, F. Pan, *J Mater. Chem. A* **2017**, *5*, 5273-5277.

[21] a) W. Zhou, L. Xue, X. Lü, H. Gao, Y. Li, S. Xin, G. Fu, Z. Cui, Y. Zhu, J. B. Goodenough, *Nano Lett.* **2016**, *16*, 7836-7841; b) W. B. Park, S. C. Han, C. Park, S. U. Hong, U. Han, S. P. Singh, Y. H. Jung, D. Ahn, K.-S. Sohn, M. Pyo, *Adv. Energy Mater.* **2018**, *8*, 1703099; c) C. Li, M. Shen, B. Hu, X. Lou, X. Zhang, W. Tong, B. Hu, *J Mater. Chem. A* **2018**, *6*, 8340-8348; d) M. Law, P. Balaya, *Energy Storage Mater.* **2018**, *10*, 102-113; e) Y. Fang, Q. Liu, L. Xiao, Y. Rong, Y. Liu, Z. Chen, X. Ai, Y. Cao, H. Yang, J. Xie, C. Sun, X. Zhang, B. Aoun, X. Xing, X. Xiao, Y. Ren, *Chem* **2018**, *4*, 1167-1180; f) W. Fang, Z. An, J. Xu, H. Zhao, J. Zhang, *RSC Adv.* **2018**, *8*, 21224-21228; g) D. Chao, C.-H. M. Lai, P. Liang, Q. Wei, Y.-S. Wang, C. R. Zhu, G. Deng, V. V. T. Doan-Nguyen, J. Lin, L. Mai, H. J. Fan, B. Dunn, Z. X. Shen, *Adv. Energy Mater.* **2018**, *8*, 1800058; h) C. Zhu, C. Wu, C.-C. Chen, P. Kopold, P. A. van Aken, J. Maier, Y. Yu, *Chem. Mater.* **2017**, *29*, 5207-5215; i) D. Wang, X. Bie, Q. Fu, D. Dixon, N. Bramnik, Y. S. Hu, F. Fauth, Y. Wei, H. Ehrenberg, G. Chen, F. Du, *Nat. Commun.* **2017**, *8*, 15888; j) J. Liu, Z. Chen, S. Chen, B. Zhang, J. Wang, H. Wang, B. Tian, M. Chen, X. Fan, Y. Huang, T. C. Sum, J. Lin, Z. X. Shen, *ACS Nano* **2017**, *11*, 6911-6920; k) Y. Zhu, L. Peng, D. Chen, G. Yu, *Nano Lett.* **2016**, *16*, 742-747; l) X. Xiang, Q. Lu, M. Han, J. Chen, *Chem. Commun.* **2016**, *52*, 3653-3656; m) J. Kim, I. Park, H. Kim, K.-Y. Park, Y.-U. Park, K. Kang, *Adv. Energy Mater.* **2016**, *6*, 1502147.

[22] a) B. Lin, S. Zhang, C. Deng, *J. Mater. Chem. A* **2016**, *4*, 2550-2559; b) K.-H. Ha, S. H. Woo, D. Mok, N.-S. Choi, Y. Park, S. M. Oh, Y. Kim, J. Kim, J. Lee, L. F. Nazar, K. T. Lee, *Adv. Energy Mater.* **2013**, *3*, 770-776.

[23] S. S. Fedotov, N. A. Kabanova, A. A. Kabanov, V. A. Blatov, N. R. Khasanova, E. V. Antipov, *Solid State Ionics* **2018**, *314*, 129-140.

[24] J. Liu, L. Yin, X.-Q. Yang, P. G. Khalifah, *Chem. Mater.* **2018**, *30*, 4609-4616.

10.1002/ange.201912964

WILEY-VCH

RESEARCH ARTICLE

Entry for the Table of Contents

RESEARCH ARTICLE

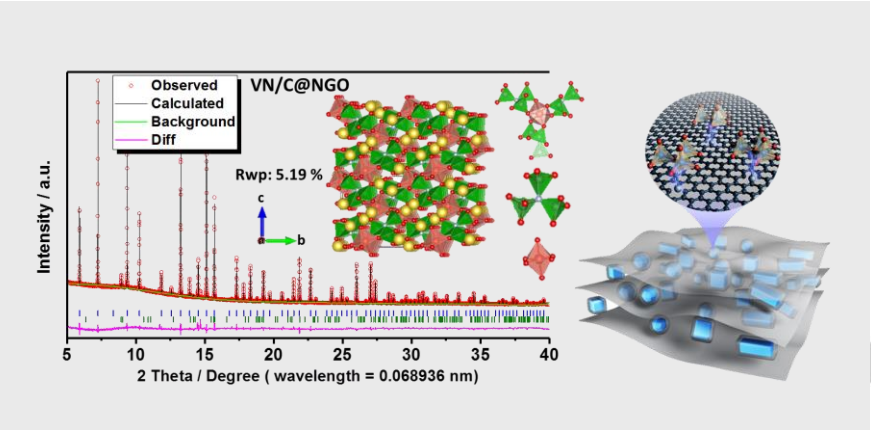

Mingzhe Chen,[+] Weibo Hua,[+] Jin Xiao, David Cortie, Xiaodong Guo, Enhui Wang, Qinfen Gu, Zhe Hu, Sylvio Indris, Xiao-Lin Wang, Shu-Lei Chou, and Shi-Xue Dou*

Page No. – Page No.

Understanding a New NASICON-Type High Voltage Cathode Material for High-Power Sodium-Ion Batteries

A newly recognized NASICON-type high-voltage cathode material of $Na_3V(PO_3)_3N$ was synthesized and its electrochemical performance was improved by carbon matrix decoration. In-depth understandings were acquired *via* in-situ XAS and in-situ XRD, and its 3D sodium pathways were clearly identified *via* DFT calculation. Its full cell performance, air/water stability indicate its strong promises for the next generation cathode material for SIBs.